Materials Horizons

ROYAL SOCIETY OF CHEMISTRY

COMMUNICATION

View Article Online
View Journal | View Issue

Check for updates

Cite this: *Mater. Horiz.*, 2023, 10, 536

Received 12th July 2022,
Accepted 19th October 2022

DOI: 10.1039/d2mh00868h

rsc.li/materials-horizons

Inorganic frameworks of low-dimensional perovskites dictate the performance and stability of mixed-dimensional perovskite solar cells†

Benny Febriansyah, [ab] Yongxin Li,[c] David Giovanni, [d] Teddy Salim, [e] Thomas J. N. Hooper, [f] Ying Sim, [bg] Daphne Ma,[e] Shoba Laxmi, [c] Yulia Lekina, [d] Teck Ming Koh, [b] Ze Xiang Shen, [d] Sumod A. Pullarkat, [c] Tze Chien Sum, [d] Subodh G. Mhaisalkar, [be] Joel W. Ager *[ah] and Nripan Mathews *[beg]

Mixed-dimensional perovskites containing mixtures of organic cations hold great promise to deliver highly stable and efficient solar cells. However, although a plethora of relatively bulky organic cations have been reported for such purposes, a fundamental understanding of the materials' structure, composition, and phase, along with their correlated effects on the corresponding optoelectronic properties and degradation mechanism remains elusive. Herein, we systematically engineer the structures of bulky organic cations to template low-dimensional perovskites with contrasting inorganic framework dimensionality, connectivity, and coordination deformation. By combining X-ray single-crystal structural analysis with depth-profiling XPS, solid-state NMR, and femtosecond transient absorption, it is revealed that not all low-dimensional species work equally well as dopants. Instead, it was found that inorganic architectures with lesser structural distortion tend to yield less disordered energetic and defect landscapes in the resulting mixed-dimensional perovskites, augmented in materials with a longer photoluminescence (PL) lifetime, higher PL quantum yield (up to 11%), improved solar cell performance and enhanced thermal stability (T_{80} up to 1000 h, unencapsulated). Our study highlights the importance of designing templating organic cations that yield low-dimensional materials with much less structural distortion profiles to be used as additives in stable and efficient perovskite solar cells.

New concepts

Addition of low-dimensional hybrid perovskites (LD HPs) into their 3D counterparts is known to result in a desirable passivation effect on the resulting "mixed-dimensional" materials. However, although there are numerous reports utilizing such an approach and despite the fact that there are many organic cations capable of templating LD HPs, many aspects remain elusive especially when it comes to the fundamental understanding of the structure–property relationship of the mixed-dimensional species derived from such different possible combinations. Using low-dimensional perovskites with contrasting inorganic framework dimensionality (2D to 0D), connectivity (flat *vs.* corrugated), and coordination deformation, this study found that higher coordination deformation surrounding the lead-iodide octahedra in the inorganic lattices (*i.e.*, intra-octahedral distortion) tends to result in worse optoelectronic properties. This observation can be explained by the fact that structural deformation tends to provide suitable environments for the formation of intra-gap states, which in turn act as recombination centers for the photogenerated charge carriers in the materials. As a result, fewer defective materials lead to devices with not only better performances, but also superior thermal stability. This study provides the previously unknown design criteria for the search of organic templating cations that can realize a material system with a much lesser defect landscape.

[a] *Berkeley Educational Alliance for Research in Singapore (BEARS), Ltd., 1 CREATE Way, Singapore, 138602, Singapore. E-mail: jwager@berkeley.edu*
[b] *Energy Research Institute at Nanyang Technological University (ERI@N), 50 Nanyang Drive, Singapore, 637553, Singapore. E-mail: nripan@ntu.edu.sg*
[c] *Chemistry and Biological Chemistry, School of Physical and Mathematical Sciences, Nanyang Technological University, 21 Nanyang Link, Singapore, 637371, Singapore*
[d] *Division of Physics and Applied Physics, School of Physical and Mathematical Sciences, Nanyang Technological University, 21 Nanyang Link, Singapore, 637371, Singapore*
[e] *School of Materials Science and Engineering, Nanyang Technological University, 50 Nanyang Avenue, Singapore, 639798, Singapore*
[f] *Centre of High Field Nuclear Magnetic Resonance (NMR) Spectroscopy and Imaging, Nanyang Technological University21 Nanyang Link, Singapore, 637371, Singapore*
[g] *Singapore-CEA Alliance for Research in Circular Economy (SCARCE), Nanyang Technological University, 62 Nanyang Drive, Singapore, 637459, Singapore*
[h] *Department of Materials Science and Engineering, University of California at Berkeley, Berkeley, California, 94720, USA*

† Electronic supplementary information (ESI) available: Crystal structures of hybrid lead-iodide perovskites (cif files). Experimental procedures, materials synthesis, additional spectra and crystallographic data (pdf). CIF data for associated crystal structures have been deposited in the Cambridge Crystallographic Data Centre under deposition numbers. CCDC 1841681, 1944784, 2169957, 2169958, and 2170085. For ESI and crystallographic data in CIF or other electronic format see DOI: **https://doi.org/10.1039/d2mh00868h**

Introduction

Hybrid halide perovskites have emerged as one of the most promising next-generation photovoltaic materials that can potentially drive down the cost of clean and renewable solar energy conversion.[1,2] Owing to their continuous three dimensional (3D) inorganic lattices comprising corner-sharing metal-halide octahedra at the molecular level, halide perovskites (HPs) possess remarkable optoelectronic properties that have propelled the certified power conversion efficiency (PCE) of the stand-alone solar cells made out of the materials to 25.7%.[3–5] For perovskite solar cells (PSCs) to be commercially viable, however, they need to endure long-term environmental stresses imposed by external stimuli, such as heat and moisture.[6] While great progress has been made in enhancing the stability of PSCs through the development of suitable packaging schemes or physical barrier layers,[7,8] the compositional variation in HPs would nonetheless determine their stability upper limit (*i.e.*, materials stability) for encapsulated devices.[9,10]

One strategy to improve the materials' stability is through dimensional engineering in which 3D HPs are mixed with hybrid metal-halide species containing lower lattice structures (*e.g.*, 2D, 1D, or even 0D) during/after the fabrication process.[11,12] Such low-dimensional (LD) materials can be considered as bulk assemblies of quantum structures where the complete isolation of inorganic metal-halide building blocks at the molecular level enables the resulting bulk materials to exhibit the intrinsic properties of individual building blocks.[4] The advantages of such structural modulation are two-fold. Firstly, in comparison to their 3D counterparts, it grants access to improved stability against degradation by moisture and oxygen as a result of the incorporation of inherently more hydrophobic, relatively bulkier organic cations.[13,14] Secondly, it affords significant room for materials exploration and engineering as the steric constraints imposed on the organic cations for the formation of 3D perovskites (typically assessed by Goldschmidt's tolerance factor) are no longer relevant.[15,16] Unfortunately, however, the utilization of LD HPs in photovoltaic applications has not been straightforward because the more confined inorganic lattices in the materials tend to result in fast charge carriers recombination, a narrow absorption window, and high excitonic binding energy, which overall would limit the current density and the PCE of the corresponding devices.[17,18] Therefore, combining 3D and LD HPs is often taken as an approach to strike the balance between efficiency and stability.

In spite of the various terminologies used in the field, the methods for realizing mixed-dimensional HPs can generally be classified into two categories:[11,12] (1) bulk incorporation of LD HPs in 3D perovskite, and (2) surface treatment of 3D perovskite with LD HPs. In the first approach, the bulky cations are typically mixed together with the 3D components in the precursor ink solution to induce the formation of LD phases throughout the bulk of the 3D perovskite during the subsequent thin film fabrication process.[19,20] Meanwhile, in the second method, the pure 3D perovskite thin film is premade before it is post-treated with orthogonal solution containing LD-templating organics, allowing a thin layer of LD species to be deposited on the surface of a 3D perovskite film.[21,22] This article focuses on the mixed-dimensional HPs in which the LD HPs are incorporated in the bulk of the 3D species.

When added in a small amount, LD HPs are known to act as an additive that provides a passivation effect to the overall materials.[23] This is made possible due to the preferential formation of the phases at the grain boundaries of the 3D HP crystallites, which reduces the amount of defects or trap states, while concurrently suppressing the ion migrations in these regions.[24,25] Such a feature is critical because it allows for improved device performance to be achieved. However, although there are numerous reports utilizing this approach and despite the fact that there are many organic cations capable of templating LD HPs, many aspects remain unknown in the fundamental understanding of the formation of mixed-dimensional species derived from such different possible combinations. In particular, it is not fully understood what factors constitute good design criteria for the organic cations when it comes to desirable device performance and stability. Given the softness and malleability of their inorganic lattices, which are considered sensitive to the local structure of the cations,[4,26] it is conceivable that tuning the organic functionalities can lead to the formation of low-dimensional species with different architectures and optoelectronic properties, which may or may not improve the overall material quality.

Results and discussion

Motivated by the above circumstances, this study aims to probe the relationships between the molecular structures of the templating organic cations, the formability of the respective LD HPs, as well as the optoelectronic properties and stability of the resulting mixed-dimensional species derived from those cations. To do that, we fabricated solar cells based on pristine 3D HPs with the $FA_{0.85}Cs_{0.15}PbI_3$ composition and n-i-p architecture where planar SnO_2 and Spiro-OMeTAD were used as electron- and hole-transporting materials, respectively (Fig. 1a, see the ESI,† for more details). We then compared the corresponding device performances with those fabricated with different solar absorber compositions, of which the 3D species are doped with 2.5 mol% of different bulky organic cations, labelled as FPEA, PyrEA, NO_2PEA, PrPyr, and NH_3PEA (Fig. 1b), to induce the formation of mixed-dimensional perovskites (refer to the ESI† for the procedure). The cations were selected based on the structural similarity with PEA (phenylethylammonium) which has commonly been used in the field. Meanwhile, 2.5 mol% (relative to 3D perovskite) was chosen because such an amount allows the presence of low-dimensional perovskites to be probed without compromising the corresponding solar cell performances (see the experimental procedure; *vide infra*). Statistical representations of individual photovoltaic parameters of 20 devices, based on

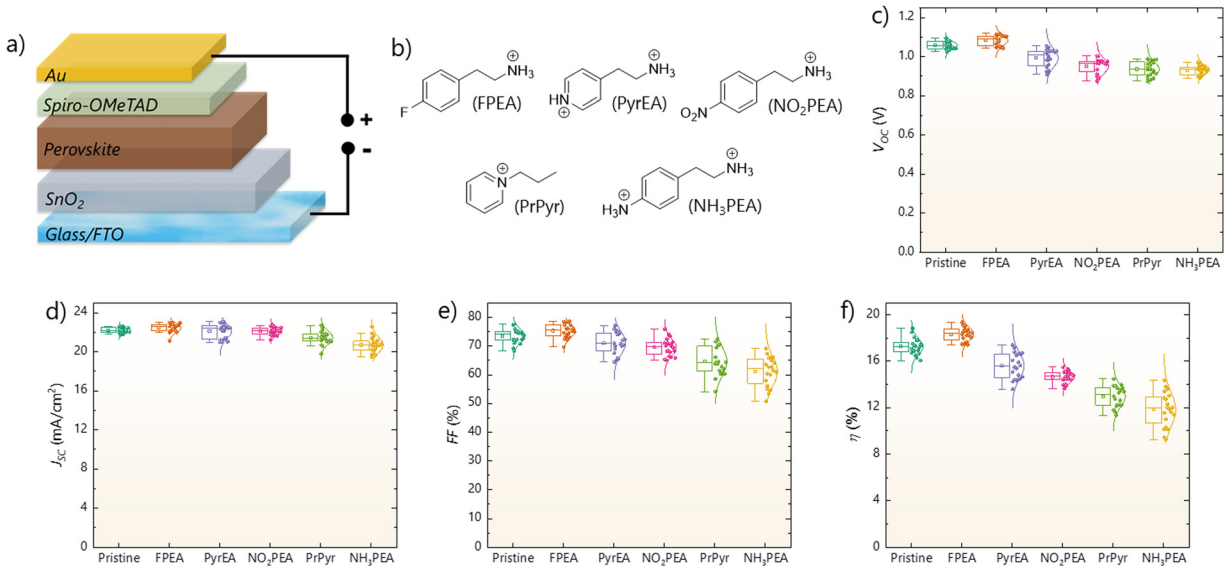

Fig. 1 (a) Schematic representation of the perovskite photovoltaic with a planar n-i-p configuration employed in this study. (b) Molecular structures of the organic cations used to template the formation of low-dimensional and mixed-dimensional halide perovskites: 4-fluorophenethylammonium (FPEA), 4-(2-ammoniumethyl)pyridinium (PyrEA), 4-nitrophenethylammonium (NO_2PEA), *N*-propyl pyridinium (PrPyr), and 4-(2-ammoniumethyl)anilinium (NH_3PEA). Statistical representations of (c) open circuit voltage (V_{OC}), (d) short-circuit current (J_{SC}), (e) fill factor (FF), and (f) power conversion efficiency (PCE or η) measured for 20 photovoltaic devices, each for pristine 3D and mixed-dimensional perovskite cells based on FPEA and NH_3PEA.

different HP variations, are depicted in Fig. 1c–f, and summarized in Tables S1–S6 (ESI†).

It can clearly be seen that not all organics result in devices with similar photovoltaic parameters and PCEs. In particular, we would like to highlight the difference between the PSCs resulting from cations FPEA and NH_3PEA. While it was possible to improve the pristine device performance by adding FPEA into the precursor solution, the devices became much less efficient with the inclusion of NH_3PEA. Specifically, pristine $FA_{0.85}Cs_{0.15}PbI_3$ solar cells have an average PCE of 17.26 ± 0.70%, while FPEA- and NH_3PEA-added samples exhibit average PCEs of 18.31 ± 0.59% and 11.84 ± 1.46, respectively. The performance improvement of the solar cells based on FPEA can be correlated with the increase in their open circuit potential (V_{OC}), where an average value of 1084 ± 27 mV was obtained, representing more than a 2% increment in comparison to that recorded for the pristine sample (1058 ± 20 mV). Meanwhile, the corresponding short-circuit current density value (J_{SC}) shows a value very close to that obtained from the control devices (average J_{SC} values of 22.43 ± 0.46 and 22.19 ± 0.28 mA cm^{-2} were observed for mixed-dimensional and 3D samples, respectively), indicating that the inclusion of bulky cation FPEA did not compromise charge transport and collection within the cells.

The current density–voltage (*J*–*V*) curves of best-performing cells under a simulated air mass (AM) of 1 Sun illumination (100 mW cm^{-2}) are further shown in Fig. S1 (ESI†) and summarized in Table S7 (ESI†) for pristine 3D and mixed-dimensional devices. Hysteresis is the major bottleneck phenomenon commonly found in the *J*–*V* curves of perovskite solar cells and originates mainly from ion migration or the presence of trap states. As shown in Fig. S1b (ESI†), the device fabricated with organic FPEA exhibited a V_{OC} of 1110 mV, J_{SC} of 22.11 mA cm^{-2}, FF of 0.79, and PCE of 19.38%, observed in the reverse scan direction, and a V_{OC} of 1100 mV, J_{SC} of 21.97 mA cm^{-2}, FF of 0.76, and PCE of 18.36% in the forward scan direction, whereas the pure $FA_{0.85}Cs_{0.15}PbI_3$ device exhibited a V_{OC} of 1090 mV, J_{SC} of 22.15 mA cm^{-2}, FF of 0.78, and PCE of 18.83% in the reverse scan direction and a V_{OC} of 1060 mV, J_{SC} of 21.47 mA cm^{-2}, FF of 0.74, and PCE of 16.84% in the forward scan direction (Fig. S1a, ESI†). The reverse scan shows enhanced V_{OC}, J_{SC}, FF, and PCE when compared to the forward scan for both mixed-dimensional and 3D perovskite devices. However, a negligible amount of hysteresis was observed in the case of the FPEA-based device compared to the pristine device, confirmed by the reduction of the hysteresis index from 0.11 (pristine) to 0.05 (FPEA-inclusion). In line with what has been reported previously,[19,24,25] we attribute the observed enhancement in V_{OC} and reduction of hysteresis behavior to the defect passivation of FPEA at the grain boundary of 3D perovskites (*vide infra*). Intriguingly, such a passivation mechanism appeared to be absent when cations PyrEA and NH_3PEA were added into the precursor solutions.

In order to explain the dependence of photovoltaic performance on different cation additives, we proceeded with investigating the structural, morphological, and optoelectronic properties of the final HP films. Measurements with UV-vis absorption spectroscopy, glancing-angle X-ray diffractometry (XRD), scanning electron microscopy (SEM) and atomic force microscopy (AFM) suggest that all the mixed-dimensional samples investigated in this study exhibit similar features to that of pristine 3D perovskite. In particular, the materials

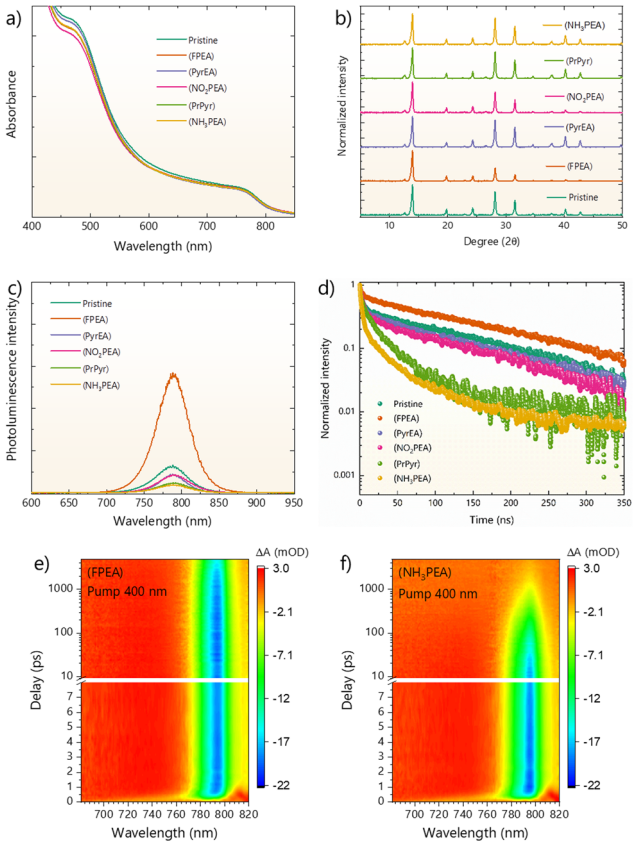

Fig. 2 (a) UV-Vis absorbance spectra, (b) glancing-angle X-ray diffractometry pattern, (c) steady-state and (d) time-resolved photoluminescence spectra of perovskite films based on 3D $FA_{0.85}Cs_{0.15}PbI_3$ and mixed-dimensional perovskites formed through the addition of cations FPEA and NH_3PEA. Pseudocolour femtosecond transition absorption plots obtained from mixed-dimensional perovskites based on cations: (c) FPEA and (d) NH_3PEA.

feature an absorption onset near 800 nm (Fig. 2a), corresponding to a band gap of around 1.54 eV (Fig. S2, ESI†), and the main XRD peak positions were attributed to, among others, the (001), (002), (012), (112), (022), and (002) HP crystallite orientations (Fig. 2b; see Table S8, ESI,† for the peak assignment). Additionally, all series of samples feature compact uniform perovskite crystallites with similar grain sizes (in the range of 400 nm; Fig. S3, ESI†) and surface roughness (of around 20 nm, Fig. S4, ESI†). While the presence of LD HP in the final materials cannot be confirmed by the aforementioned techniques (as we note that features such as XRD peaks at low angles below 10° and a plate-like morphology that have previously been reported in other studies due to the presence of low-dimensional species in the films are absent in our system,[13] *vide infra*), the results signify that the main phases are heavily dominated by the 3D species and the final amount of LD HP is very small and does not significantly affect the continuous lattice framework of $FA_{0.85}Cs_{0.15}PbI_3$.

Interestingly, however, the photoluminescence quantum yield (PLQY) and charge carrier dynamics (as determined by time-resolved PL and femtosecond transition absorption experiments) profiles do vary across different mixed-dimensional samples. In particular, mixed-dimensional HP based on FPEA emits a photon at 795 nm around one order of magnitude higher in terms of intensity than that of NH_3PEA (Fig. 2c and Table S9, ESI†), while simultaneously showing an enhanced fluorescence lifetime (Fig. 2d; the average characteristic decay times of NH_3PEA- and FPEA-added samples were observed to be 10 ns and 120 ns, respectively; see Table S10 (ESI†) for the fitting details and values for the TRPL of different mixed-dimensional perovskites investigated in this study). A similar trend was also observed in the corresponding transient absorption spectra of the thin films with the inclusion of FPEA in comparison to that with NH_3PEA where the latter shows a more pronounced photo-bleaching peak band in the 795 nm spectral region (Fig. 2e and f; see Fig. S5, ESI,† for the corresponding peak fitting and its explanation). The increase in PL intensity and carrier lifetime lengthening indicate that in contrast to other mixed-dimensional perovskites fabricated with PyrEA and NH_3PEA, non-radiative recombination channels are relatively reduced in the FPEA-based sample. The observations also suggest that although there is little variation in terms of structural and morphological aspects, the energetic and defect landscapes among the five mixed-dimensional HPs appear to be different, and corroborating this observation with the V_{OC} data of the corresponding solar cells presented previously, it can be concluded that defect passivation could only be achieved with cation FPEA, but not with PyrEA to NH_3PEA.

While attempting to elucidate the factors that determine the optoelectronic contrast observed in the series of our mixed-dimensional materials, we assume that the previously reported findings, in which the low-dimensional species was identified to be located at the grain boundaries of the 3D perovskites,[11,12] also hold true in our system. If that's the case, we hypothesize that the optoelectronic characteristics at the grain boundaries would then affect the overall material quality. This would also mean that such a characteristic is highly dependent on the selectivity of the bulky cations in directing certain low-dimensional metal-halide frameworks. This is because, although the templating organics possess frontier orbitals not capable of "interacting" with those of inorganic lattices, their specific molecular arrangement (*e.g.*, charge distribution, steric level, and weak interactions) can lead to the formation of a wide range of anionic metal-halide fine structures featuring different energetic and defect landscapes.[4,11,26] As such, in order to analyze the cations templating effect, we proceeded with the growth of single crystals of pure low-dimensional hybrids based on the respective organics FPEA and NH_3PEA and had the structures solved through the single crystal X-ray diffraction technique.

Unsurprisingly, as presented in Fig. 3, we found that, indeed, the different cations direct the formation of HPs with varying types of inorganic motifs. While 2D layered architectures were obtained with FPEA, PyrEA, and NO_2PEA, polymeric 1D chain and discrete mononuclear coordination complexes (*i.e.*, "0D") resulted from PrPyr and NH_3PEA, respectively. Even within the 2D category itself, different metal-halide connectivity

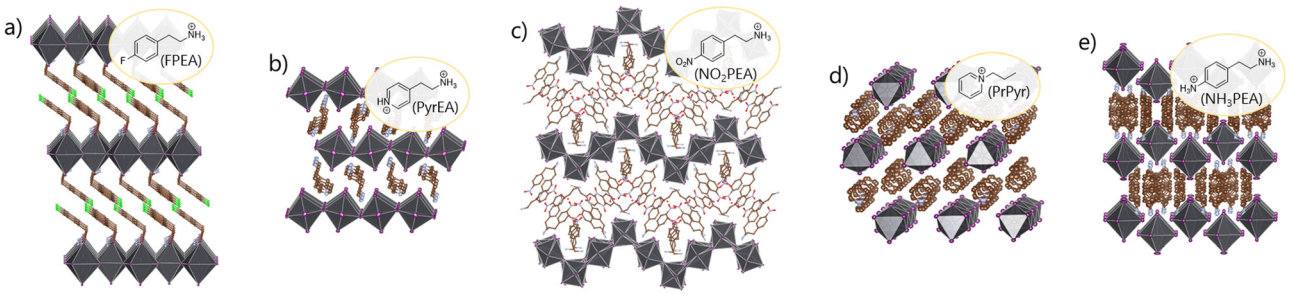

Fig. 3 X-Ray crystal structures of (a) (100) 2D perovskite ("Ruddlesden–Popper") $(FPEA)_2PbI_4$, (b) (100) 2D perovskite ("Dion–Jacobson") $(PyrEA)PbI_4$, (c) (110) 2D perovskite $(NO_2PEA)_2PbI_4$, (d) 1D "perovskite" $(PrPyr)PbI_3$, and (e) 0D "perovskite" $(NH_3PEA)_2PbI_6$. Ellipsoids are shown at 50% probability. H atoms are omitted for clarity. Gray, purple, brown, red, and blue spheroids represent Pb, I, C, O, and N atoms, respectively. The insets show the molecular structures of the templating cations.

or topology can be observed: the "flat" $(FPEA)_2PbI_4$ and $(PyrEA)PbI_4$ represent the "(100)" subclass (though the former is a typical "Ruddlesden–Popper" type and the latter is of "Dion–Jacobson" variant), while $(NO_2PEA)_2PbI_4$ is an example of the comparatively rarer corrugated "(110)" 2D perovskite. The formation of different perovskites has serious implications for the corresponding optoelectronic properties. This is because as mentioned previously, the physical nature of the resulting hybrids is dictated mainly by their inorganic halometallate components with connectivity, dimensionality and disorder playing major roles,[4,26] which, in turn, are sensitive to the metal-halide second-sphere coordination environment surrounding the metal-halide octahedra.[27,28]

For the above reason, we are interested in examining the different degrees of lead-iodide coordination deformations in the pure LD HPs based on FPEA and NH_3PEA and probing its interdependence on the optoelectronic features of the corresponding mixed-dimensional materials and devices. Relevant to our investigation, it has previously been demonstrated that intra-octahedral distortion can determine the defectivity of the material *via* modulation of the defect formation energies.[27,29] In particular, it was observed that higher intra-octahedral distortion tends to give rise to the higher formation of intra-gap states as a result of a lower barrier for hole self-trapping which stabilizes the formation of trihalide species like I_3^-. Such charge localization could be detrimental to the materials and device performance. The degree of lead-iodide coordination deformation in this study is accessed by using three structural parameters, namely octahedral bond length distortion (Δ_{oct}), octahedral elongation (λ_{oct}), and octahedral angle variance (σ^2_{oct}).[30–33] The equations for each parameter and explanations of their meaning can be found in the ESI,† while a summary is given in Table 1. The resulting values take into account the lead-iodide bond length and angle deformations in their $[PbI_6]^{4-}$ octahedra building blocks, where larger values indicate a greater degree of distortion (see Tables S11–S20, ESI† for the list of bond lengths and angles of the inorganic component in each of the LD HPs).

Generally, it is found that the lower the dimensionality of the inorganic lattices, the higher the distortion. Although it has to be examined on a case-by-case basis, we associate this trend with the higher exposure of the inorganic network to the crystal packing forces (provided by the cations in the form of coulombic and hydrogen bonding interactions) when the dimensionality is reduced, which makes the lead coordination sphere susceptible to deviation from the ideal octahedral symmetry. In addition, across different 2D perovskites, "Dion–Jacobson" and corrugated structures appear to have a higher distortion in comparison to that of the "Ruddlesden–Popper" variant. The large intra-octahedral distortion in the "Dion–Jacobson"-type of material is owing to the inherently asymmetric environment of their constituent $[PbI_6]^{4-}$ octahedra in which the dicationic PyrEA within the monolayer alternate in terms of its orientation, with either its phenyl head or ethylammonium tail pointing into the "bay regions" formed by the terminal iodide ligands of four nearest neighbouring Pb–I octahedra (Fig. 3b). Meanwhile, the presence of two types of alternating octahedra in $(NO_2PEA)_2PbI_4$ (*i.e.*, those with *trans*- and *cis*-oriented terminally bound iodides, respectively) as a result of supramolecular interactions with organic NO_2PEA is the origin to the significant deformation within the $[PbI_6]^{4-}$ coordination (Fig. 3c).

The difference in the structural profiles of each of the LD HPs is also manifested in the Raman spectra of each of the species. As presented in Fig. S6a (ESI†), the low wavenumber Raman bands are mainly contributed by the vibrations of the inorganic sub-lattices. The peaks above 60–70 cm^{-1} are associated with Pb–I bond stretching coupled with the libration or translation vibrations of the organic molecules, while the

Table 1 Distortion parameters derived from the single crystal X-ray structures of low-dimensional perovskites based on cations FPEA and NH_3PEA

Compound	Δd^b ($\times 10^4$)	$\lambda_{oct}{}^c$	$\sigma^2_{oct}{}^d$
$(FPEA)_2PbI_4$	0.58	1.0013	4.29
$(PyrEA)PbI_4$	1.54	1.0038	12.96
$(NO_2PEA)_2PbI_4{}^a$	6.15	1.0065	21.53
$(PrPyr)PbI_3$	7.90	1.0108	36.15
$(NH_3PEA)_2PbI_6$	23.23	1.0028	1.41

[a] Averaged distortion parameters are given for $(NO_2PEA)_2PbI_4$ as it contains three geometrically distinct octahedra. [b] Octahedral bond length distortion. [c] Octahedral elongation. [d] Octahedral angle variance.

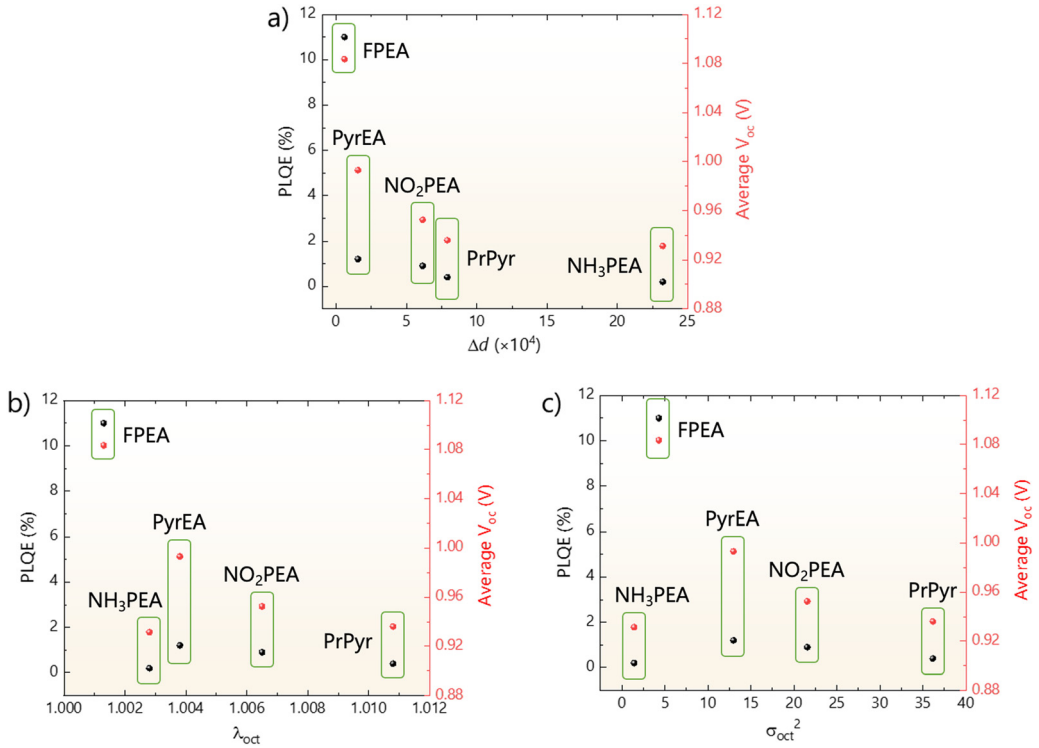

Fig. 4 Correlation plots between intra-octahedral distortion parameters: (a) octahedral bond length distortion (extracted from Table 1), (b) octahedral elongation (Table 1), and (c) octahedral angle variance (Table 1) obtained from pure low-dimensional perovskites based on cations FPEA and NH_3PEA with the photoluminescence quantum yield (PLQY; Table S9, ESI†) and average open-circuit voltage (V_{OC}) recorded from mixed-dimensional perovskites with the addition of cations FPEA and NH_3PEA (Tables S2–S6, ESI†).

bands above 110 cm^{-1} are mainly induced by organic librations.[34–36] The peaks below 60 cm^{-1} are further assigned to the bending, twisting and distortion in the iodoplumbate network which vary across the materials depending on the extent of propagation of the $[PbI_6]^{4-}$ building blocks in the material lattices, thus forming fingerprint regions. A more detailed discussion regarding the Raman feature of the series of LD HPs investigated in this study can be found in the ESI.†

We then attempted to correlate the lead-iodide coordination deformation of pure LD HPs templated by cations FPEA and NH_3PEA with the V_{OC} and PLQY data obtained from the corresponding mixed-dimensional materials and interestingly, a close relationship can be observed between them (Fig. 4). In general, it was found that higher distortion tends to result in worse optoelectronic properties. As hypothesized earlier, this can be explained by the fact that structural deformation tends to provide suitable environments for the formation of intra-gap states, which in turn act as recombination centers for the photogenerated charge carriers in the materials.[27,29] Therefore, adding those cations in the 3D system results in more defective materials, rather than passivating them. This trend resonates with the recently reported work in light emitting devices, where the more distorted perovskites would give rise to worse performing devices.[37] More intriguingly, we observed that this structural distortion parameter appears to outcompete other factors, such as inorganic lattice separation, when it comes to improving the device PCE. As shown in Fig. 3, $(PyrEA)PbI_4$ features a much shorter Pb–I interlayer distance than $(FPEA)_2PbI_4$. While the shorter separation may be beneficial for charge transport, the resulting mixed-dimensional perovskite still suffers from the more disordered energetic landscapes as a consequence of the heavier coordination deformation experienced by the $[PbI_6]^{4-}$ octahedra in the lattices templated by PyrEA.

In order to rule out the electronic effect of the cation's functionality, we also fabricated devices and performed structural analysis on the LD HPs based on PEA and 4-hydroxyphenylethylammonium (OHPEA). As shown in Fig. S7 and Tables S21, S22 (ESI†), the device performances are not affected by the electron withdrawing or donating capabilities of the groups attached to the phenyl rings, but rather it is the nature of the resulting inorganic lattices that causes the fluctuations. Featuring relatively milder intra-octahedral distortion relative to the compound based on NH_3PEA, the best performing devices of PSCs whose active layers were fabricated with the addition of PEA and OHPEA could still achieve 19.03% and 18.53%, respectively (champion device of the NH_3PEA-doped sample is 14.35% efficient). We believe that this empirical observation could explain why PEA, for example, has consistently been used by many research groups as effective performance enhancers over the years.

Furthermore, we also observed that crystallization kinetics play little role in determining the quality of the final material. We performed the *in situ* UV-vis absorption spectroscopy

experiment (see the ESI† for the details) and found that mixed-dimensional samples have similar features to that of pristine 3D $FA_{0.85}Cs_{0.15}PbI_3$. In particular, the majority of peaks (at 355, 420, 529, 779 nm) that appeared right after the anti-solvent was introduced were effectively from those of 3D perovskites (Fig. S8, ESI;† black arrows), while there seems to be no contribution from the low-dimensional species, at least in our measurement timescale, that would otherwise have appeared at 319, 376, and 524 nm for the FPEA-based sample and at 305 and 371 nm for the NH_3PEA-based sample (Fig. S8, ESI;† dotted blue line). This can be attributed to the relatively small amount of bulky organic dopants that was added to the starting precursor solution. Nonetheless, although it was difficult to trace the kinetics, solid-state nuclear magnetic resonance (ss-NMR) spectra of the scratched thin film powder (Fig. S9; see the ESI† for experimental details) confirm the presence of low-dimensional perovskites at the end of the crystallization process and surprisingly, the amount is pretty much similar in terms of the ratio in comparison to that in the starting ink solution (*i.e.*, around 2.5 mol% of LD HPs relative to the 3D $FA_{0.85}Cs_{0.15}PbI_3$). Moreover, though it is harder to probe if the multiple-layered structures formed in the final materials, it can be confirmed from ss-NMR spectra that the bulky organic cations exist in an LD HP form, rather than segregating into iodide salt (Fig. S9b, ESI†).

Having known which system was more defective relative to the others, it became more straightforward to predict what the stability trend would look like. As expected, upon carrying out stability monitoring at 85 °C with 10% relative humidity (RH), mixed-dimensional HPs doped with cation FPEA exhibited much better stability in comparison to that of NH_3PEA (Fig. S10, ESI†). In particular, while more than 50% of the active material had converted to PbI_2 in the case of NH_3PEA (as suggested from the respective XRD patterns of the aged samples), mixed-dimensional HP based on FPEA could retain around 80% of the initial amount even after 1000 hours of testing. Indeed, the stability behaviour of FPEA also outcompeted that of pristine $FA_{0.85}Cs_{0.15}PbI_3$ where the active material was only left with *ca.* 60% under the same measurement timeframe. Such a similar trend resonated with what was observed in the device and optical studies, suggesting that higher quality 3D perovskites would last longer when subjected to durability testing. This is particularly true because while the presence of bulky cations could render the overall materials to be more hydrophobic (thus more stable towards moisture), we were intrigued to find that the thermal stability of LD HPs alone

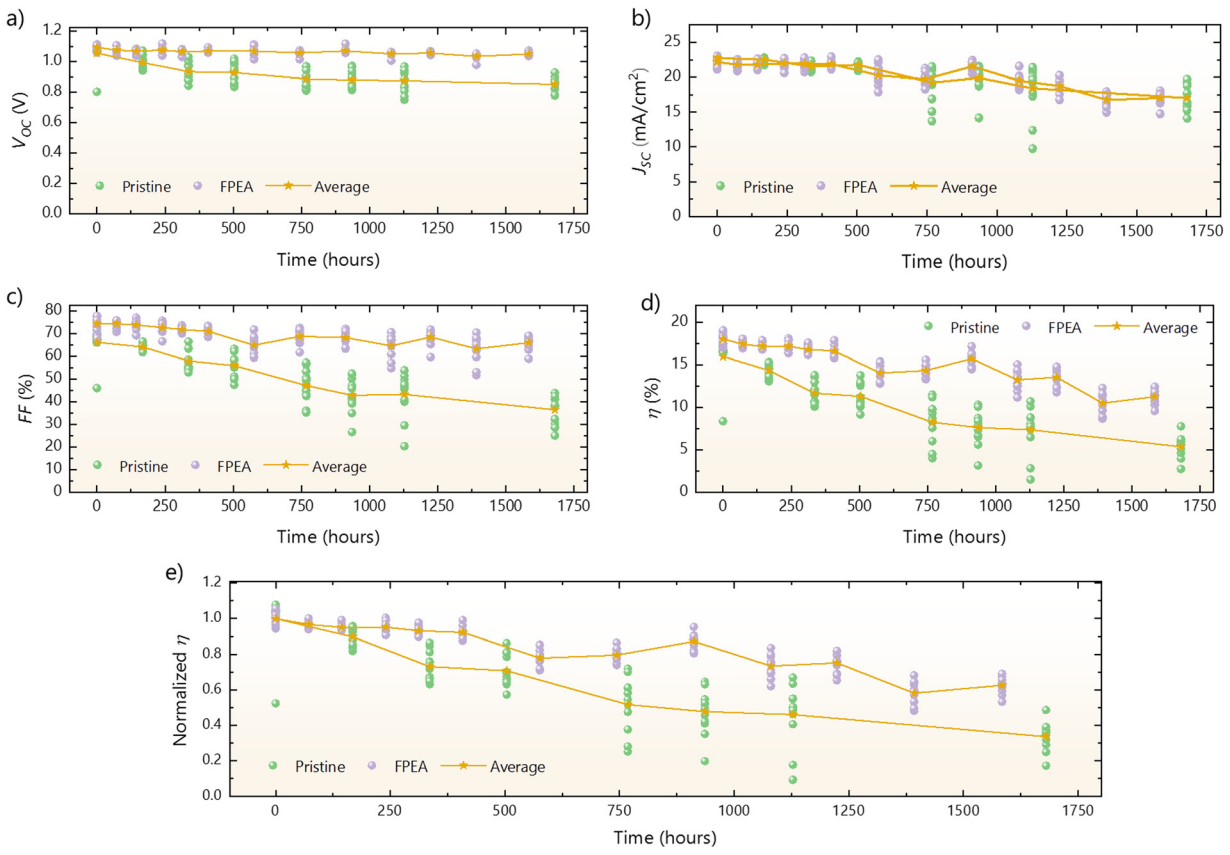

Fig. 5 Thermal-stability test comparison between the pristine 3D $FA_{0.85}Cs_{0.15}PbI_3$ and mixed-dimensional perovskite solar cells based on the cation FPEA. Tests were performed for more than 1500 hours at a relative humidity (RH) level of 10% where the photovoltaic parameters namely (a) open circuit voltage (V_{OC}), (b) short-circuit current (J_{SC}), (c) fill factor (FF), and (d) power conversion efficiency (PCE or η) were regularly monitored. The black arrows indicate improvement made by the addition of cation FPEA in the composition. (e) Normalized PCE parameters at different time intervals.

was actually lower than the pure 3D counterparts (Fig. S11, ESI†). As such, we reaffirm the role of LD HPs as additives capable of passivating defects, especially at the grain boundaries, without causing radical changes to the overall material's structural and physical properties (which are significantly 3D in nature).

More stable materials subsequently translated to PSCs with better thermal stability. When subjected to a similar environment (85 °C; 10% RH), as presented in Fig. 5, T_{80} of the unencapsulated devices based on FPEA improved by a factor of ~4 relative to that of their pure 3D counterparts. Despite the use of relatively thermally unstable Spiro-OMeTAD in our current architecture, mixed-dimensional PSCs with FPEA still exhibited an average PCE of 11.28 ± 0.80%, even after subjecting them for more than 1500 hours. Therefore, this result demonstrates the benefit of significantly improving the material stability of the solar absorbers and we foresee even much better stability behaviour when a polymer-based HTL and/or a physical barrier/encapsulant are utilized in the device stack.[7,8,38] Taking a closer look at each of the photovoltaic characteristics collected throughout the stability testing, the more significant improvement in FPEA-added devices seems to come from the fill factor, indicating that the degradation process could have initiated at the interfaces. This applies especially in our case because not only moisture is capable of inducing the perovskite degradation, but the hygroscopic and volatile additives added in the HTL layer could also play a role.[39,40]

We then performed depth profiling X-ray photoelectron spectroscopy (XPS) to gain further insight into the potential cross-sectional compositional difference between mixed-dimensional and pristine 3D perovskites. Interestingly, we did observe a non-homogeneous distribution of the bulky organic cations in the film. As shown in Fig. 6a, the XPS signal corresponding to cation FPEA was only observed in the early stage of scanning. As a comparison, we also performed the same experiment with the film of $FA_{0.85}Cs_{0.15}PbI_3$ that has been post-treated with FPEA (*i.e.*, spin-coating the cation after the pristine 3D perovskite was fabricated; see the ESI† for details). The resulting sample exhibited a higher XPS signal of FPEA due to the relatively more amount that ended up in the film during deposition. However, a similar trend can be observed: the signal would eventually disappear after subsequent etching of the film (Fig. 6b). More interestingly, we found that similar behavior was also demonstrated by organics with different functionalities. In the case of cation NH_3PEA, for example, we observed the strongest XPS peak only at the initial stage of the etching process (Fig. 6c and d). Though a further study is required to understand the principle behind the process, our initial examination implies that the phenomenon could be universal and not only the fluorinated group causes the organic species to be "repelled" to the top of the films.

We suggest that the above observation could be related to the kinetics of formation of the low-dimensional species which, in comparison to that of 3D counterparts, appears to be relatively more preferable under fast crystallization that occurs during the spincoating process. This is in line with the report by Zhou and co-workers who found that the composition of mixed-dimensional halide perovskite thin films right after spincoating consisted of more of the layered halide perovskites featuring low "n" values (*e.g.*, n = 2 and n = 3 where n denotes the number of contiguous 2D inorganic layers, *i.e.*, not separated by organic cations) rather than their 3D counterparts.[41] This indicates the preferred formation of low-dimensional halide perovskites templated by bulky organic cations at the early stage of crystallization, despite the formation energy of the materials being in general higher than that of their 3D counterparts.[42] We anticipate that such a tendency can play an important role especially when a HTL with volatile or reactive dopants, such as Spiro-OMeTAD, is utilized and a judiciously designed bulky cation is expected to improve the stability of multi-dimensional HP-based devices even more.

Conclusions

In summary, we investigated the effects of the functional groups of structurally related organic cations on the formability of the corresponding low-dimensional hybrid perovskites

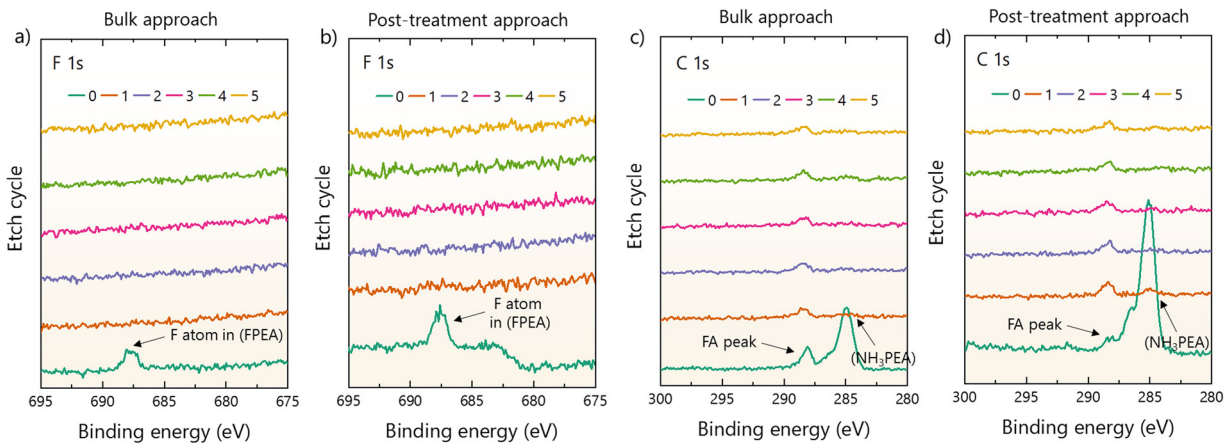

Fig. 6 Depth profiling profiles of mixed-dimensional perovskite samples based on bulky cations FPEA and NH_3PEA fabricated *via* bulk (a and c) and post-treatment (b and d) approaches. The plots are constructed from high resolution XPS spectra of the F 1s (for FPEA-based sample, (a and b)) and C 1s (for NH_3PEA-based samples, (c and d)) collected on several etch cycles.

together with the optoelectronic and stability behaviors of mixed-dimensional species resulting from their mixing with 3D $FA_{0.85}Cs_{0.15}PbI_3$. Generally, it is found that higher coordination deformation surrounding the lead-iodide octahedra in inorganic lattices (*i.e.*, intra-octahedral distortion) tends to result in worse optoelectronic properties (*e.g.*, short photoluminescence (PL) lifetime, low PL quantum yield and open-circuit potential). This observation can be explained by the fact that structural deformation tends to provide suitable environments for the formation of intra-gap states, which in turn act as recombination centers for the photogenerated charge carriers in the materials. Less defective materials lead to devices with not only better performances (more than 19% PCE), but also superior thermal stability. (T_{80} up to 1000 h, unencapsulated). A closer look at the samples' cross sectional compositional profiles suggests a non-homogeneous distribution of the bulky organic cations in the film in which more of the species are found near the surface of the perovskite layer. This behavior is observed regardless of the functionality attached to the organic cores, implying that the templating capability of the bulk cations could also play important roles in modulating the interfacial stability of the device stacks, especially when a HTL with volatile or reactive dopants, such as Spiro-OMeTAD, is utilized.

Conflicts of interest

The authors declare the following competing financial interest(s): two of the authors, N. M. and S. M., are the directors of Prominence Photovoltaics Pte Ltd., a perovskite solar cell commercialization company.

Acknowledgements

The authors would like to acknowledge funding from the Singapore National Research Foundation through the Intra-CREATE Collaborative Grant (NRF2018-ITC001-001), Energy Innovation Research Program (NRF2015EWT-EIRP003-004 and Solar CRP: S18-1176-SCRP), and MOE Tier 2 project MOE2019-T2-2-097. The authors would also like to acknowledge the Center of High Field NMR Spectroscopy and Imaging at Nanyang Technological University for the use of their facilities.

References

1 M. Gratzel, The light and shade of perovskite solar cells, *Nat. Mater.*, 2014, **13**(9), 838–842.
2 N.-G. Park and K. Zhu, Scalable fabrication and coating methods for perovskite solar cells and solar modules, *Nat. Rev. Mater.*, 2020, **5**(5), 333–350.
3 Best Research-Cell Efficiencies, Rev.30-06-2022 (NREL,2022); https://www.nrel.gov/pv/assets/pdfs/best-research-cell-efficiencies-rev220630.pdf.
4 B. Saparov and D. B. Mitzi, Organic-Inorganic Perovskites: Structural Versatility for Functional Materials Design, *Chem. Rev.*, 2016, **116**(7), 4558–4596.
5 T. C. Sum and N. Mathews, Advancements in perovskite solar cells: photophysics behind the photovoltaics, *Energy Environ. Sci.*, 2014, **7**(8), 2518–2534.
6 M. V. Khenkin, E. A. Katz, A. Abate, G. Bardizza, J. J. Berry, C. Brabec, F. Brunetti, V. Bulović, Q. Burlingame, A. Di Carlo, R. Cheacharoen, Y.-B. Cheng, A. Colsmann, S. Cros, K. Domanski, M. Dusza, C. J. Fell, S. R. Forrest, Y. Galagan, D. Di Girolamo, M. Grätzel, A. Hagfeldt, E. von Hauff, H. Hoppe, J. Kettle, H. Köbler, M. S. Leite, S. Liu, Y.-L. Loo, J. M. Luther, C.-Q. Ma, M. Madsen, M. Manceau, M. Matheron, M. McGehee, R. Meitzner, M. K. Nazeeruddin, A. F. Nogueira, Ç. Odabaşı, A. Osherov, N.-G. Park, M. O. Reese, F. De Rossi, M. Saliba, U. S. Schubert, H. J. Snaith, S. D. Stranks, W. Tress, P. A. Troshin, V. Turkovic, S. Veenstra, I. Visoly-Fisher, A. Walsh, T. Watson, H. Xie, R. Yıldırım, S. M. Zakeeruddin, K. Zhu and M. Lira-Cantu, Consensus statement for stability assessment and reporting for perovskite photovoltaics based on ISOS procedures, *Nat. Energy*, 2020, **5**(1), 35–49.
7 K. A. Bush, A. F. Palmstrom, Z. J. Yu, M. Boccard, R. Cheacharoen, J. P. Mailoa, D. P. McMeekin, R. L. Z. Hoye, C. D. Bailie, T. Leijtens, I. M. Peters, M. C. Minichetti, N. Rolston, R. Prasanna, S. Sofia, D. Harwood, W. Ma, F. Moghadam, H. J. Snaith, T. Buonassisi, Z. C. Holman, S. F. Bent and M. D. McGehee, 23.6%-efficient monolithic perovskite/silicon tandem solar cells with improved stability, *Nat. Energy*, 2017, **2**(4), 17009.
8 L. Shi, M. P. Bucknall, T. L. Young, M. Zhang, L. Hu, J. Bing, D. S. Lee, J. Kim, T. Wu, N. Takamure, D. R. McKenzie, S. Huang, M. A. Green and A. W. Y. Ho-Baillie, Gas chromatography-mass spectrometry analyses of encapsulated stable perovskite solar cells, *Science*, 2020, **368**(6497), eaba2412.
9 S.-H. Turren-Cruz, A. Hagfeldt and M. Saliba, Methylammonium-free, high-performance, and stable perovskite solar cells on a planar architecture, *Science*, 2018, **362**(6413), 449–453.
10 Y. Deng, S. Xu, S. Chen, X. Xiao, J. Zhao and J. Huang, Defect compensation in formamidinium–caesium perovskites for highly efficient solar mini-modules with improved photostability, *Nat. Energy*, 2021, **6**(6), 633–641.
11 G. Grancini and M. K. Nazeeruddin, Dimensional tailoring of hybrid perovskites for photovoltaics, *Nat. Rev. Mater.*, 2018, **4**(1), 4–22.
12 M. A. Mahmud, T. Duong, J. Peng, Y. Wu, H. Shen, D. Walter, H. T. Nguyen, N. Mozaffari, G. D. Tabi, K. R. Catchpole, K. J. Weber and T. P. White, Origin of Efficiency and Stability Enhancement in High-Performing Mixed Dimensional 2D-3D Perovskite Solar Cells: A Review, *Adv. Funct. Mater.*, 2021, **32**(3), 2009164.
13 Z. Wang, Q. Lin, F. P. Chmiel, N. Sakai, L. M. Herz and H. J. Snaith, Efficient ambient-air-stable solar cells with 2D–3D heterostructured butylammonium-caesium-formamidinium lead halide perovskites, *Nat. Energy*, 2017, **2**(9), 17135.
14 B. Chaudhary, T. M. Koh, B. Febriansyah, A. Bruno, N. Mathews, S. G. Mhaisalkar and C. Soci, Mixed-

Dimensional Naphthylmethylammoinium-Methylammonium Lead Iodide Perovskites with Improved Thermal Stability, *Sci. Rep.*, 2020, **10**(1), 429.

15 J. Xue, R. Wang, X. Chen, C. Yao, X. Jin, K.-L. Wang, W. Huang, T. Huang, Y. Zhao, Y. Zhai, D. Meng, S. Tan, R. Liu, Z.-K. Wang, C. Zhu, K. Zhu, M. C. Beard, Y. Yan and Y. Yang, Reconfiguring the band-edge states of photovoltaicperovskites by conjugated organic cations, *Science*, 2021, **371**(6529), 636–640.

16 C. Liu, Y. Yang, K. Rakstys, A. Mahata, M. Franckevicius, E. Mosconi, R. Skackauskaite, B. Ding, K. G. Brooks, O. J. Usiobo, J. N. Audinot, H. Kanda, S. Driukas, G. Kavaliauskaite, V. Gulbinas, M. Dessimoz, V. Getautis, F. De Angelis, Y. Ding, S. Dai, P. J. Dyson and M. K. Nazeeruddin, Tuning structural isomers of phenylenediammonium to afford efficient and stable perovskite solar cells and modules, *Nat. Commun.*, 2021, **12**(1), 6394.

17 B. Febriansyah, Y. Lekina, B. Ghosh, P. C. Harikesh, T. M. Koh, Y. Li, Z. Shen, N. Mathews and J. England, Molecular Engineering of Pure 2D Lead-Iodide Perovskite Solar Absorbers Displaying Reduced Band Gaps and Dielectric Confinement, *ChemSusChem*, 2020, **13**(10), 2693–2701.

18 L. N. Quan, M. Yuan, R. Comin, O. Voznyy, E. M. Beauregard, S. Hoogland, A. Buin, A. R. Kirmani, K. Zhao, A. Amassian, D. H. Kim and E. H. Sargent, Ligand-Stabilized Reduced-Dimensionality Perovskites, *J. Am. Chem. Soc.*, 2016, **138**(8), 2649–2655.

19 J. W. Lee, Z. Dai, T. H. Han, C. Choi, S. Y. Chang, S. J. Lee, N. De Marco, H. Zhao, P. Sun, Y. Huang and Y. Yang, 2D perovskite stabilized phase-pure formamidinium perovskite solar cells, *Nat. Commun.*, 2018, **9**(1), 3021.

20 T. Zhou, H. Lai, T. Liu, D. Lu, X. Wan, X. Zhang, Y. Liu and Y. Chen, Highly Efficient and Stable Solar Cells Based on Crystalline Oriented 2D/3D Hybrid Perovskite, *Adv. Mater.*, 2019, **31**(32), e1901242.

21 Q. Jiang, Y. Zhao, X. Zhang, X. Yang, Y. Chen, Z. Chu, Q. Ye, X. Li, Z. Yin and J. You, Surface passivation of perovskite film for efficient solar cells, *Nat. Photonics*, 2019, **13**(7), 460–466.

22 J. Joseph Yeow Wan Foong, B. Febriansyah, P. Jyoti Singh Rana, T. Ming Koh, D. Jun Jie Tay, A. Bruno, S. Mhaisalkar and N. Mathews, Effects of All-Organic Interlayer Surface Modifiers on the Efficiency and Stability of Perovskite Solar Cells, *ChemSusChem*, 2021, **14**(6), 1524–1533.

23 F. Zhang and K. Zhu, Additive Engineering for Efficient and Stable Perovskite Solar Cells, *Adv. Energy Mater.*, 2019, **10**(13), 1902579.

24 D. S. Lee, J. S. Yun, J. Kim, A. M. Soufiani, S. Chen, Y. Cho, X. Deng, J. Seidel, S. Lim, S. Huang and A. W. Y. Ho-Baillie, Passivation of Grain Boundaries by Phenethylammonium in Formamidinium-Methylammonium Lead Halide Perovskite Solar Cells, *ACS Energy Lett.*, 2018, **3**(3), 647–654.

25 X. Wang, K. Rakstys, K. Jack, H. Jin, J. Lai, H. Li, C. S. K. Ranasinghe, J. Saghaei, G. Zhang, P. L. Burn, I. R. Gentle and P. E. Shaw, Engineering fluorinated-cation containing inverted perovskite solar cells with an efficiency of >21% and improved stability towards humidity, *Nat. Commun.*, 2021, **12**(1), 52.

26 H. Lin, C. Zhou, Y. Tian, T. Siegrist and B. Ma, Low-Dimensional Organometal Halide Perovskites, *ACS Energy Lett.*, 2017, **3**(1), 54–62.

27 B. Febriansyah, T. Borzda, D. Cortecchia, S. Neutzner, G. Folpini, T. M. Koh, Y. Li, N. Mathews, A. Petrozza and J. England, Metal Coordination Sphere Deformation Induced Highly Stokes-Shifted, Ultra Broadband Emission in 2D Hybrid Lead-Bromide Perovskites and Investigation of Its Origin, *Angew. Chem., Int. Ed.*, 2020, **59**(27), 10791–10796.

28 L. Mao, Y. Wu, C. C. Stoumpos, M. R. Wasielewski and M. G. Kanatzidis, White-Light Emission and Structural Distortion in New Corrugated Two-Dimensional Lead Bromide Perovskites, *J. Am. Chem. Soc.*, 2017, **139**, 5210–5215.

29 D. Cortecchia, S. Neutzner, A. R. Srimath Kandada, E. Mosconi, D. Meggiolaro, F. De Angelis, C. Soci and A. Petrozza, Broadband Emission in Two-Dimensional Hybrid Perovskites: The Role of Structural Deformation, *J. Am. Chem. Soc.*, 2017, **139**(1), 39–42.

30 N. W. Thomas, Crystal Structure-Physical Property Relationships in Perovskites, *Acta Crystallogr., Sect. B: Struct. Sci.*, 1989, **45**, 337–344.

31 M. W. Lufaso and P. M. Woodward, Jahn-Teller distortions, cation ordering and octahedral tilting in perovskites, *Acta Crystallogr., Sect. B: Struct. Sci.*, 2004, **60**(Pt 1), 10–20.

32 K. Robinson, G. V. Gibbs and P. H. Ribbe, Quadratic Elongation: A Quantitative Measure of Distortion in Coordination Polyhedra, *Science*, 1971, **172**, 567–570.

33 J. A. Alonso, M. J. Martínez-Lope, M. T. Casais and M. T. Fernández-Díaz, Evolution of the Jahn–Teller Distortion of MnO_6 Octahedra in $RMnO_3$ Perovskites (R = Pr, Nd, Dy, Tb, Ho, Er, Y): A Neutron Diffraction Study, *Inorg. Chem.*, 2000, **39**(5), 917–923.

34 M. A. Pérez-Osorio, Q. Lin, R. T. Phillips, R. L. Milot, L. M. Herz, M. B. Johnston and F. Giustino, Raman Spectrum of the Organic–Inorganic Halide Perovskite $CH_3NH_3PbI_3$ from First Principles and High-Resolution Low-Temperature Raman Measurements, *J. Phys. Chem. C*, 2018, **122**(38), 21703–21717.

35 N. S. Dahod, A. France-Lanord, W. Paritmongkol, J. C. Grossman and W. A. Tisdale, Low-frequency Raman spectrum of 2D layered perovskites: Local atomistic motion or superlattice modes?, *J. Chem. Phys.*, 2020, **153**(4), 044710.

36 C. Quarti, G. Grancini, E. Mosconi, P. Bruno, J. M. Ball, M. M. Lee, H. J. Snaith, A. Petrozza and F. D. Angelis, The Raman Spectrum of the $CH_3NH_3PbI_3$ Hybrid Perovskite: Interplay of Theory and Experiment, *J. Phys. Chem. Lett.*, 2014, **5**(2), 279–284.

37 N. F. Jamaludin, B. Febriansyah, Y. F. Ng, N. Yantara, M. Li, D. Giovanni, J. Fu, Y. B. Tay, T. Baikie, T. C. Sum, N. Mathews and S. Mhaisalkar, Molecular design of two-dimensional perovskite cations for efficient energy cascade in perovskite light-emitting diodes, *Appl. Phys. Lett.*, 2021, **119**(15), 154101.

38 G. Kim, H. Min, K. S. Lee, D. Y. Lee, S. M. Yoon and S. I. Seok, Impact of strain relaxation on performance of α-formamidinium lead iodide perovskite solar cells, *Science*, 2020, **370**(6512), 108–112.

39 Y. Li, Y. Wang, T. Zhang, S. Yoriya, P. Kumnorkaew, S. Chen, X. Guo and Y. Zhao, Li dopant induces moisture sensitive phase degradation of an all-inorganic $CsPbI_2Br$ perovskite, *Chem. Commun.*, 2018, **54**, 9809–9812.

40 Y. Cho, H. Ohkita, Y. Li, J. Bing, J. Zheng, S. Huang and A. Ho-baillie, The Effect of 4-tert-Butylpyridine Removal on Efficiency and Thermal Stability in Perovskite Solar Cells, *J. Photopolym. Sci. Technol.*, 2019, **32**, 5.

41 N. Zhou, Y. Shen, L. Li, S. Tan, N. Liu, G. Zheng, Q. Chen and H. Zhou, Exploration of Crystallization Kinetics in Quasi Two-Dimensional Perovskite and High Performance Solar Cells, *J. Am. Chem. Soc.*, 2018, **140**, 459.

42 L. N. Quan, M. Yuan, R. Comin, O. Voznyy, E. M. Beauregard, S. Hoogland, A. Buin, A. R. Kirmani, Z. Zhao, A. Amassian, D. H. Kim and E. H. Sargent, Ligand-Stabilized Reduced-Dimensionality Perovskites, *J. Am. Chem. Soc.*, 2016, **138**, 2649.

